Macroscale assembly of peptide nanotubes†‡

Kun Lu,[a] Liang Guo,[b] Anil K. Mehta,[a] W. Seth Childers,[a] Steven N. Dublin,[c] S. Skanthakumar,[d] Vincent P. Conticello,[a] P. Thiyagarajan,[b] Robert P. Apkarian[c] and David G. Lynn*[a]

Received (in Cambridge, UK) 23rd January 2007, Accepted 11th April 2007
First published as an Advance Article on the web 30th April 2007
DOI: 10.1039/b701029j

Simple oligopeptides that self-assemble into homogeneous nanotubes can be directed to further assemble into macroscale parallel arrays through protein "salting out" strategies.

Aβ(16–22), CH_3CO-KLVFFAE-NH_2, the amphiphilic, cationic core segment of the Alzheimer's disease peptide, assembles into micron long highly homogeneous hollow tubes at pH 2.[1] These tubes have a 52 nm cross-sectional diameter and are bounded by thin 4 nm walls (Fig. 1A). The peptides in the wall adopt a β-sheet conformation[1] and are positively charged in solution due to the protonated terminal amine on the lysine side chains. The tubes can be densely coated with negatively charged colloidal gold nanoparticles establishing that positive charges are localized to the peptide nanotube surface,[2] a feature preventing nanotube self-association. In this report we demonstrate that the cationic nature of the nanotubes can be further exploited by inducing the nanotubes to assemble into robust lamellar supramacromolecular filaments.

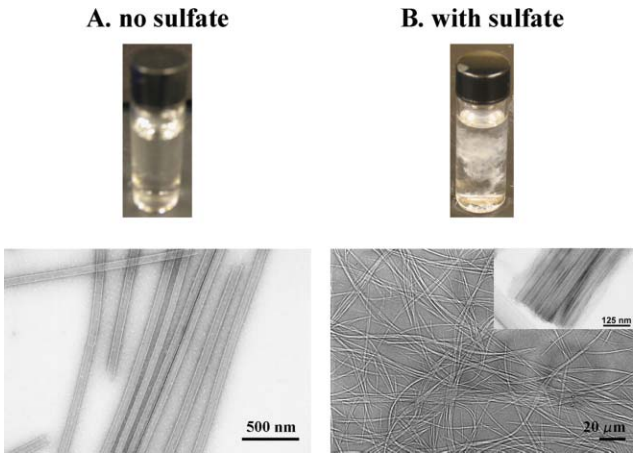

Fig. 1 Sulfate-induced axially aligned peptide nanotube macrofilaments. (A) 2.6 mM Aβ(16–22) in 40% acetonitrile–water with 0.1% TFA (pH 2) self-assembles into highly homogeneous, soluble peptide nanotubes as measured by transmission electron microscopy (lower panel TEM). On drying, these tubes flatten to a width of 80 nm. (B) Upon addition of Na_2SO_4, the peptide nanotubes coalesce into macrofilaments, maintaining an average width of ~1 μm as shown in the optical micrograph. (B lower panel inset) TEM micrograph of the macrofilaments shows the well-aligned nanotubes of the bundles.

Salt-induced precipitation is widely used for purification of charged proteins[3] and can also precipitate amyloid fibrils.[4] The precipitation strongly depends on the ion's position[5] in the Hofmeister series, where SO_4^{2-} is efficient for precipitating positively charged proteins.[6] The addition of Na_2SO_4, K_2SO_4 or H_2SO_4 to a solution of the Aβ(16–22) nanotubes results in the immediate formation of visible white filaments (Fig. 1B). This phenomenon is independent of cation identity and monovalent anions, including Cl^-, NO_3^-, and $H_2PO_4^-$, were significantly less effective, although some nanotube bundling was seen above NaCl concentrations of 3M. Optical microscopy indicates an average filament diameter of ~1 μm and a contour length of >5 mm (Fig. 1B). TEM shows the macrofilaments to be composed of axially aligned nanotubes (Fig. 1B, inset), and IR analysis (data not shown) identified tightly bound sulfate ions sequestered within the bundles. IR, X-ray and electron diffraction analyses found little difference in peptide conformation between the nanotubes and the macroscopic bundles, confirming the characteristic cross-β conformation typical of amyloids (see Fig. S1 in ESI‡).[7,8]

The macroscopic assembly and nanotube organization within the hydrated bundles was further investigated using small angle X-ray scattering (SAXS) at the 12-ID beam-line of Argonne National Laboratory's Advanced Photon Source. Aliquots of Na_2SO_4 or NaCl from 18 mM stock solutions were added step-wise to 400 μL of a 2.6 mM Aβ(16–22) nanotube solution and SAXS was measured at room temperature 30 min after each titration. The scattering pattern of the neat peptide solution (Fig. 2A, no salt) was consistent with the hollow cylindrical form factor for individual nanotubes with an outer diameter of 52 nm.[1] Upon addition of 3.6 mM sulfate, strong peaks appear consistent with the structure factor of organized nanotubes. The first and higher order peaks have significantly greater intensity and are shifted to lower Q (Fig. 2A, left). With increasing salt concentration, peak intensities monotonically increase and above 9 mM the scattering pattern remains unchanged. However, no such scattering patterns were observed upon sodium chloride titration (Fig. 2B).

As the scattering pattern represents the product of the nanotube form factor and spatial correlation of the nanotubes that form

[a]*Center for the Analysis of Supramolecular Self-assemblies, Departments of Chemistry and Biology, Emory University, Atlanta, Georgia 30322, USA. E-mail: david.lynn@emory.edu*
[b]*Intense Pulsed Neutron Source, Argonne National Laboratory Argonne, Illinois 60439, USA*
[c]*Integrated Microscopy and Microanalytical Facility, Emory University, Atlanta, Georgia 30322, USA*
[d]*Chemistry Division, Argonne National Laboratory Argonne, Illinois 60439, USA*

† In memoriam: Robert Phillip Apkarian (1953–2006) colleague and friend.

‡ Electronic supplementary information (ESI) available: XRD of peptide nanotubes and sulfate bundled nanotubes and comparison of derived structure factors for nanotubes in salt solutions using form factors for a core–shell cylinder and a rectangular cross-section cylinder. See DOI: 10.1039/b701029j

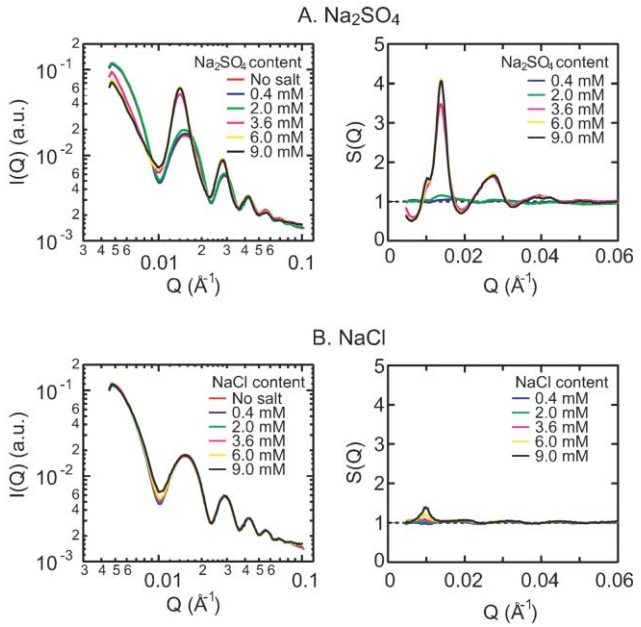

Fig. 2 SAXS as a function of salt concentration. Na_2SO_4 (A) and NaCl (B) solutions (18 mM) were titrated into 400 μL of a peptide nanotube solution self-assembled from 2.6 mM Aβ(16–22) in 40% acetonitrile–water containing 0.1% TFA (pH 2). Left: Scattering intensity normalized to the peptide concentration. Right: Structure factors obtained for each salt concentration by dividing the normalized scattering data for salt solutions by that for the neat peptide solution.

bundles, we extracted the structure factors of the nanotube bundles by dividing the normalized SAXS data of the peptide in Na_2SO_4 solutions by the SAXS data of the neat peptide solution normalized for peptide concentration and contrast. The obtained structure factors for peptides in salt solutions are shown on the right panel of Fig. 2A. The first order diffraction peak at Q* = 0.0138 (1/Å), corresponding to a *d*-spacing of 45.6 nm (2π/Q*), is significantly smaller than the initial nanotube diameter of 52.0 nm. The higher order peaks at 2Q* and 3Q* are consistent with lamellar rather than the hexagonal packing normally expected for the assembly of rod-like objects. We validated the lamellar order in the macrofilaments by also using a form factor for a nanotube with a square cross-section consistent with a width of 45.6 nm (see Fig. S2 in ESI‡). The SAXS data provides evidence that sulfate ions induce a sharp concentration-dependent bundling of the nanotubes into highly ordered lamellar-like macrofilaments.

Maximizing the surface contacts between rod-shaped tubes is likely to distort the 4 nm walls. These thin-walled peptide nanotubes appear robust and malleable, as shown by the flattened nanotubes in the dehydrated TEM images (Fig. 1A). Moreover, a height of twice the wall thickness observed in atomic force microscopy images[1] is consistent with flattened tubes where the water in the internal cavity of the tube has been expelled. Nanotubes assembled by surfactant-like peptides[9] display a range of twists and folded morphologies, again suggesting flexible wall structures. Thus, the repeat distance of 45.6 nm observed by SAXS for the bundles may arise from subtle distortions of the tubes to maximize tube-tube interaction. Geometrically, a 52 nm circular cross-section tube can be shaped into a square cross-section with 4 rounded corners and flat sides of length 23.4 nm as depicted in

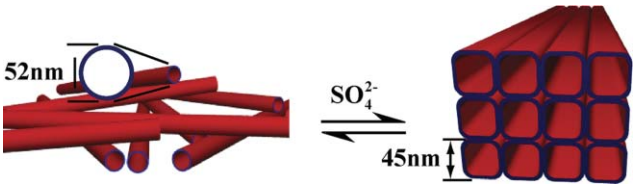

Fig. 3 Schematic of the sulfate-directed peptide nanotube aggregation into lamellar-like arrays. Left: Peptide nanotube surfaces are positively charged (drawn in red) and hence repulsive, leading to a random distribution in solution with a homogeneous diameter of 52 nm and wall thickness of 4 nm (inset). The hydrophobic peptide core is coloured blue. Right: Sulfate ions stabilize the 45.6 nm wide nanotubes that are deformed to have flat walls by tube–tube contacts, resulting in linear arrays of tubes with non-hexagonal packing.

Fig. 3. Cryo-etch high-resolution scanning electron microscopy (cryo-etch HRSEM) images from flash-frozen solutions reveal randomly distributed flexible nanotubes (Fig. 4, top). Upon the addition of sulfate, the nanotubes axially align with ends that can appear remarkably ordered (Fig. 4, bottom). Close examination of the macrofilament cross-section indeed reveals that the nanotubes

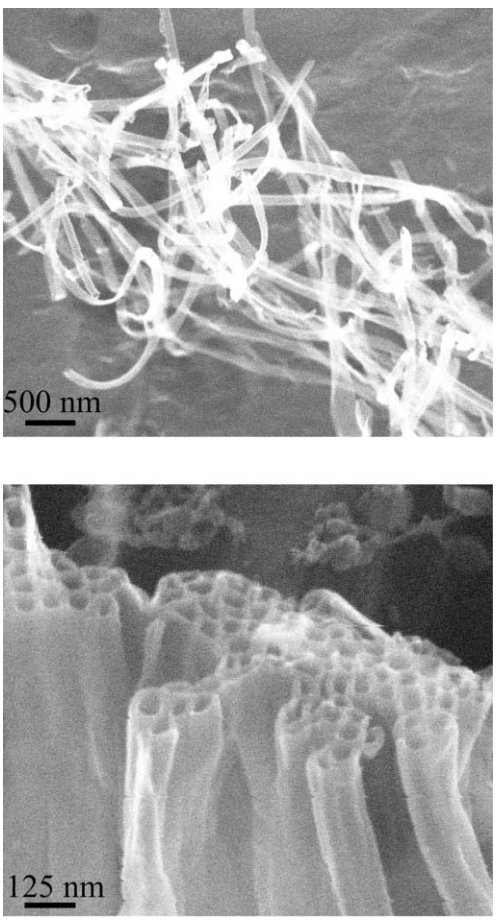

Fig. 4 Cryo-etch high-resolution scanning electron microscopy (cryo-etch HRSEM) images of chromium sputter-coated Aβ(16–22) peptide nanotubes before (top) and after (bottom) sulfate bundling. Within these reversibly forming macroassemblies, the nanotubes are deformed with non-circular cross-sections maximizing the contact surface-area through lamellar-like packing (bottom).

are deformed to maximize surface contact (Fig. 4, bottom) and display regions of both lamellar- and hexagonal-like packing. The flash-freezing of the cryo-etch HRSEM process provides a snapshot of this structure, but the solution SAXS data, which allows interrogation of the entire sample, indicates that these nanotubes pack in lamellar arrays.

Although the mechanism for salt-induced protein aggregation remains poorly understood,[6] anions are generally believed to screen electrostatic repulsion between positively charged peptide assemblies and induce short-range colligative forces. Monte Carlo simulations of positively charged spherical colloidal particles in aqueous electrolyte solutions, as models for ion–ion and ion–protein interactions, ion-polarizability, and an approximate representation of the solvent,[10] suggest that maximum attraction between the charged surfaces occurs when buffered by a monolayer of counter-ions. This attraction is predicted to be greater in the presence of divalent anions due to a reduced entropic loss from binding.[11] The sulfate anion induced nanotube bundling is consistent with these predictions, where tube-to-tube surface association is mediated by counter-ions.

These data establish a strategy to induce soluble homogeneous peptide nanotubes to undergo higher order self-assembly. While peptide assemblies have been induced to form hydrogels as hexagonal arrays,[12] the ordering of Aβ(16–22) into bundles of ordered lamellar nanotubes is remarkable. The flexibility, cross-sectional dimensions, and nature of the surface of the peptide nanotube wall strongly influence the architecture of these macroscale assemblies. Molecular sculpting into higher ordered microscale assemblies requires control of both peptide self-assembly into tubes and directed association of peptide nanotubes. Therefore, the simple and well known ion "salting out" represents a general approach to control higher order self-assembly of nanoscale objects. As this assembly is reversible, the degree of kinetic and thermodynamic control that can now be achieved will define the utility of these materials as robust templates for generating even higher order functional macroassemblies.

VPC and DGL thank DOE ER15377 and Emory Neurology Microscopy Core Laboratory. DGL and PT thank the Packard Foundation Interdisciplinary Science Program (99–8327) for financial support. This work benefited from use of the Chemistry Division, IPNS and 12-ID at APS, funded by the U.S. DOE, BES under contract number DE-AC02-06CH11357 to the University of Chicago.

Notes and references

1 K. Lu, J. Jacob, P. Thiyagarajan, V. P. Conticello and D. G. Lynn, *J. Am. Chem. Soc.*, 2003, **125**, 6391–6393.
2 K. Lu, V. P. Conticello and D. G. Lynn, Templating Colloidal Metal Nanoparticle Assemblies: Use of the Aβ Amyloid Peptide Nanotube, in *Proteins as Materials*, ed. V. P. Conticello, A. Chilkoti, E. Atkins and D. G. Lynn (Mater. Res. Soc. Symp. Proc. 826E, Warrendale, PA), 2004, V1.6.1–V1.6.6.
3 R. K. Scopes, *Protein purification: principles and practice*, 3rd edn., Springer Verlag, New York, 1994.
4 P. E. Fraser, J. T. Nguyen, D. T. Chin and D. A. Kirschner, *J. Neurochem.*, 1992, **59**, 1531–1540.
5 F. Hofmeister, *Arch. Exp. Pathol. Pharmackol.*, 1888, **24**, 247–260.
6 K. D. Collins, *Methods*, 2004, **34**, 300–311.
7 A. J. Geddes, K. D. Parker, E. D. Atkins and E. Beighton, *J. Mol. Biol.*, 1968, **32**, 343–358.
8 P. Sikorski, E. D. Atkins and L. C. Serpell, *Structure*, 2003, **11**, 915–926.
9 S. Vauthey, S. Santoso, H. Gong, N. Watson and S. Zhang, *Proc. Natl. Acad. Sci. U. S. A.*, 2002, **99**, 5355–5360.
10 F. W. Tavares, D. Bratko, A. Striolo, H. W. Blanch and J. M. Prausnitz, *J. Chem. Phys.*, 2004, **120**, 9859–9869.
11 R. J. Bacquet and P. J. Rossky, *J. Phys. Chem.*, 1988, **92**, 3604–3612.
12 C. Valery, M. Paternostre, B. Robert, T. Gulik-Krzywicki, T. Narayanan, J. C. Dedieu, G. Keller, M. L. Torres, R. Cherif-Cheikh, P. Calvo and F. Artzner, *Proc. Natl. Acad. Sci. U. S. A.*, 2003, **100**, 10258–10262.